Thermal investigation of relaxations of interacting and non-interacting amorphous solid dispersions

Anna Péter-Haraszti[1] · Petra Záhonyi[1] · Attila Farkas[1] · István Csontos[1] · Zsombor Kristóf Nagy[1] · Edina Szabó[1] ·
Guy Van den Mooter[2] · György Marosi[1]

Abstract

In the present research, thermal investigation of amorphous solid dispersions (ASDs) was performed in order to compare their relaxation transitions. Two different active pharmaceutical ingredients (APIs), namely naproxen (NAP) and spironolactone (SPIR), were used as model drugs and combined with polyvinylpyrrolidone vinyl acetate (PVPVA64) copolymer to form stable ASDs. The reason for the API selection was their different interacting potentials based on the presence (in the case of NAP) and the lack of H-bond donor group (in the case of SPIR). Determination of both T_g and sub-T_g transitions suggested that ASDs containing NAP and PVPVA64 are 'interacting' systems with respect to the H-bonding. Besides, temperature-dependent Raman spectroscopic experiments confirmed that the naphthalene ring of the NAP has a significant role in the sub-T_g relaxations. In contrast, SPIR-PVPVA64 systems proved to be 'non-interacting' ASDs according to the MDSC, TSDC, and Raman measurements. This study highlights that the combination of the results of different thermoanalytical investigations with spectroscopic methods helps to understand the molecular background of the relaxations in ASDs and thus contributes to the conscious design of stable amorphous pharmaceuticals in the early stage of development.

Keywords Amorphous solid dispersion · Molecular mobility · Relaxation transitions · Stability · Intermolecular hydrogen bond

Introduction

Pharmaceutical amorphous solid dispersions (ASDs) have great potential in the field of formulation development as the dissolution and the bioavailability of poorly water-soluble active pharmaceutical ingredients (APIs) are enhanced using these systems [1]. Although the number of approved ASD-loaded medicines is increasing year by year, their development and authorization are more challenging due to their complex physical behavior [2]. For their regulatory approval, it must be proven that the ASD remains not only chemically but also physically stable until the expiration date, meaning that the API's crystallization begins neither during the manufacturing nor during the storage and usage [3]. Therefore, understanding the correlations between the measurable properties and physical stability of ASDs is essential to the conscious design of this kind of formulations [4].

Among the physical descriptors of ASDs, the glass transition temperature (T_g) is one of the most decisive parameters in terms of stability [5]. Above the T_g, the amorphous parts behave elastically and viscously, and greater movements between the molecules can be observed [6]. In an amorphous state, intensive segment motions in different ways can lead to crystallization [7, 8] which can result in decreased dissolution and bioavailability [3]. It is often observed that ASD systems characterized by a lower T_g are generally more unstable [9]. A usually mentioned rule is that the T_g of the given ASD must be 50 °C above the

✉ Edina Szabó
  szabo.edina@vbk.bme.hu

✉ Guy Van den Mooter
  guy.vandenmooter@kuleuven.be

[1] Department of Organic Chemistry and Technology, Faculty of Chemical Technology and Biotechnology, Budapest University of Technology and Economics, Műegyetem rkp. 3, Budapest 1111, Hungary

[2] Department of Pharmaceutical and Pharmacological Sciences, Drug Delivery and Disposition, KU Leuven, Campus Gasthuisberg ON2, Herestraat 49 b921, 3000 Leuven, Belgium

maximum storage temperature to be able to ensure the stable form of the amorphous system [10]. However, it is important to note that different excipients (polymers) or the preparation methods can result in variations in molecular mobility, intermolecular interactions, and physical structure, which can in turn affect the T_g of the material [11]. Furthermore, it is essential to consider that there can be substantial differences between the T_g values of the APIs and polymers used in ASDs. Amorphous APIs have low T_g in general and thus usually poor stability in the amorphous state at room temperature [12], while the widely used polymers can be characterized with higher T_g values [13]. T_g of the resulting ASD is located between the T_g values of the components, depending on the percentage composition by mass, the possible secondary interactions [14]. Based on this, a polymer with a high T_g is worth choosing, which can 'antiplasticize' the API and stabilize the ASD system [15]. Furthermore, with regard to polymer selection, the drug-polymer interactions also need to be kept in mind. Interactions of different strengths can change the T_g and the molecular mobility of the ASD, thereby affecting the stability of the developed system [16, 17]. It could be expected that ASD systems with stronger second-order interactions between the API and the polymer forming will have greater physical stability [18].

In addition to the T_g (usually called α-relaxation in the case of amorphous materials), it is worth discussing the relaxation processes at lower temperatures (generally mentioned as sub-T_g transitions). Closest to T_g is the β-relaxation, above which the movement of certain bonds can be observed, but below this, even these parts behave more rigidly [19]. At an even lower temperature, other sub-T_g processes can be observed, where only molecular movements can happen [20]. Although sub-T_g relaxations mean only very small molecular motions, this mobility can also affect the stability of the amorphous form. This was investigated by Kissi et al. [21], who found that a better correlation can be observed between the stability of pure amorphous drugs and β-relaxation temperature ($T_β$) than with the T_g. The APIs with higher $T_β$ were more stable while the neat amorphous drugs with lower $T_β$ recrystallized in a shorter time. Sibik et al. made similar observations; in their work, amorphous indomethacin with higher $T_β$ was stable at 298

K for 7 days, while paracetamol and flufenamic acid characterized by lower $T_β$ values were stable only for 1 day [22]. Sub-T_g relaxations show a correlation with the stability not only in pure amorphous APIs but also in ASDs as well. Grzybowska et al. found that different drug-polymer interactions in celecoxib-loaded ASDs resulted in differences in the sub-T_g relaxations, which indicated a clear correlation with the stability of the investigated systems [23].

As both T_g and sub-T_g transitions can have a decisive role in the stability of amorphous pharmaceuticals, measuring these properties of ASDs is essential during the development and manufacturing of this kind of medicines. Determination of the T_g is already a common practice in the pharmaceutical industry for characterizing amorphous materials, and usually, different thermoanalytical methods are used for this purpose [24]. The most widely used technique for measuring the T_g is the differential scanning calorimetry (DSC) or its upgraded version, the modulated DSC (mDSC) [25, 26]. However, there are many other methods for the determination of T_g, such as dielectric relaxation spectroscopy (DRS), thermally stimulated depolarization current (TSDC), micro thermal analysis, and dynamic mechanical analysis (DMA) [27–30]. These techniques are applicable for determining sub-T_g transitions as well. For example, in the work of Kissi et al. [21], DMA was used for determining the β-relaxation temperature while terahertz spectroscopy [22], DRS [31], and TSDC method [32] proved to be also suitable for detecting sub-T_g transitions of amorphous drugs. Detecting sub-T_g transitions is challenging as the minor molecular movements give only very weak signals [21]. Therefore, it can be useful to perform comprehensive thermoanalytical investigations to better understand the stability-related behavior of complex amorphous pharmaceuticals [27].

Proceeding on the track of the previous studies, this research aims to examine the relaxation temperatures of two different API-polymer systems with different methods such as DSC and TSDC. The two APIs used for this purpose were naproxen (NAP) and spironolactone (SPIR), while poly(vinylpyrrolidone-*co*-vinyl acetate) (PVPVA64) served as the polymer matrix in both cases (Fig. 1). The reason for the selection of these model systems was to investigate the molecular mobility of 'strongly interacting' and

Fig. 1 Chemical structures of NAP (**a**), PVPVA64 (**b**), and SPIR (**c**). Red circles represent the hydrogen-bond acceptor parts, while the blue frame shows the molecule's hydrogen-bond donor parts
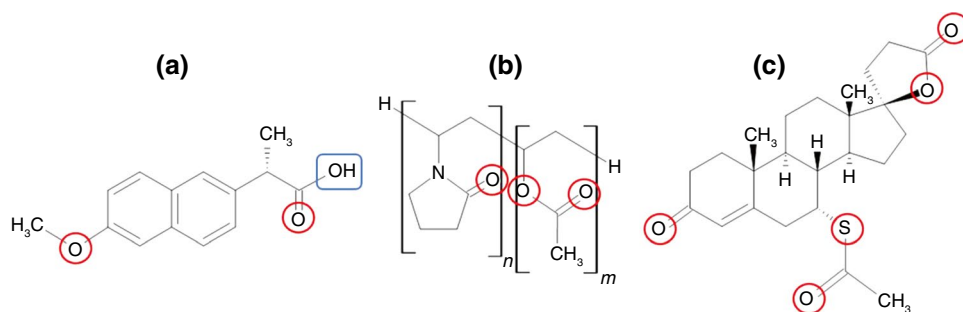
'less interacting' or possibly 'non-interacting' ASDs. In other words, the effect of a strong secondary interaction, the hydrogen bond (H-bond), was explored in the context of the T_g and sub-T_g relaxations. The ASDs containing NAP and PVPVA64 demonstrated the 'strongly interacting' systems because this API has a H-bond donor hydroxyl group, which allows the formation of intermolecular H-bond with the polymer. In contrast, no H-bonding, just weaker van der Waals interactions, can occur in the case of ASDs containing SPIR and PVPVA64 ('less interacting' or 'non-interacting' systems) since both materials only have H-bond acceptor groups.

Besides, the comparison of the relaxation behavior of 'strongly interacting' and 'less interacting' or 'non-interacting' ASDs, another goal was to investigate the molecular units that are involved in the relaxations. For this purpose, Raman spectroscopy was already used in the case of certain polymers for examining their relaxation temperatures [33, 34]. To the best of the authors' knowledge, no publication can be found in the literature, in which Raman spectroscopic method and TSDC analysis were applied for investigating sub-T_g transitions of pharmaceutical ASDs. However, simultaneous application of these techniques can help the in-depth understanding of the molecular mobility of these complex systems, as the critical parts of the molecules might be visible. Consequently, temperature-dependent Raman spectroscopic and TSDC measurements can support the design of stable ASDs in the pharmaceutical industry.

Materials and methods

Materials

NAP (Fig. 1a) was obtained from J&K Scientific Ltd. (Lommel, Belgium), while micronized SPIR Form II (Fig. 1c) was received from Gedeon Richter Plc. (Budapest, Hungary). PVPVA64 (Kollidon® VA64) (Fig. 1b) was purchased from BASF (Ludwigshafen, Germany). Dichloromethane (DCM) and absolute ethanol (EtOH) were supplied from Merck Ltd.

Methods

Preparation of amorphous solid dispersions

Single-needle electrospinning (SNES) method with an NT-35 high-voltage direct current supply (MA2000; Unitronik Ltd., Nagykanizsa, Hungary) and a 0.5-mm inner diameter nozzle was used for the preparation of the ASDs of PVPVA64 and NAP or SPIR. A voltage of 20 kV was applied to the needle while a grounded collector was placed opposite to that. The nozzle-collector distance was set to 15 cm during all experiments. A SEP-10S Plus type syringe

pump (Aitecs, Vilnius, Lithuania) was applied for dosing the solutions to the tip of the needle, and the feeding rates were set to 10 mL h^{-1} and 8 mL h^{-1} in the case of NAP-loaded and SPIR-loaded solvents, respectively. All ASD systems were produced at room temperature (25 °C) and about $45 \pm 5\%$ relative humidity. Samples containing 10, 20, 30, 40, and 50% API were prepared using a 1:1 mixture of DCM and EtOH. The amount of the polymer was fixed to 2000 mg/8 mL and 2500 mg/8 mL in the case of NAP-loaded and SPIR-loaded samples, respectively.

Modulated differential scanning calorimetry (MDSC)

The MDSC examinations were performed with a Mettler Toledo DSC3 + device (Mettler Toledo AG, Zürich, Switzerland) in TOPEM® (stochastic temperature-modulated) mode. The temperature was increased from 0 to 250 °C with 2 °C min^{-1} total heating rate, meanwhile the modulation was ± 0.5 °C and the modulation frequency changed randomly between 15 and 30 s. Dry nitrogen with a flow rate of 50 mL h^{-1} was used for purging the chamber. For each measurement, approximately 8–10 mg sample was weighed into a 40-μL aluminum pan with a pierced lid. For measuring the T_g of the amorphous SPIR, the starting temperature was adjusted to − 20 °C, and the sample was prepared in situ in the equipment via quench cooling. After that, the temperature was increased to 250 °C while the same heating rate and modulation were used as in the case of the electrospun samples. The upper temperature limit allowed identifying the possible melting and decomposition of the samples.

The theoretical T_g values of the ASDs ($T_{g,mix}$) were determined based on the Gordon–Taylor method (Eq. 1) and the T_g of the pure components measured by MDSC. In Eq. (1), $T_{g,d}$ and $T_{g,p}$ indicate the T_g of the drug and the polymer, respectively. The w character in Eq. (1) refers to the mass fraction of the components, while ρ in Eq. (2) means the density of the drug and the polymer.

$$T_{g,mix} = (w_d T_{g,d} + K w_p T_{g,p})/(w_d + K w_p) \tag{1}$$

$$K \approx \rho_d T_{g,d}/\rho_p T_{g,p} \tag{2}$$

Thermally stimulated depolarization current (TSDC)

The TSDC experiments were performed with a TSCII-type thermally stimulated current equipment (Setaram, Calure, France) connected with a Norhof 910 LN2 pump (Ede, The Nederlands), which controlled the coolant. The device was cooled by liquid nitrogen thus not only the T_g, but the sub-T_g relaxations were possible to be investigated as well. Before each measurement, the measuring chamber was purged

with helium three times to get an inert atmosphere to avoid noises.

For T_g determination, approximately 20 mg fibrous ASD sample was measured into a copper sample holder bounded by a Teflon ring (Fig. 2a). After compressing the measured sample manually, a stainless-steel disk was put on the smooth surface of the ASD (Fig. 2b). With this process, samples with a thickness of ca. 0.5 mm were prepared. During the experiments, the same measuring method and process parameters (annealing temperature, $T_a = 20$ °C, annealing time, $t_a = 1$ min, polarization temperatures, $T_p =$ approximately 10–20 °C higher than the T_g of the given sample determined by DSC, polarization time, $t_p = 5$ min, field strength, $E = 300$ V mm^{-1}, temperature range between 0 (T_0) and 150 °C (T_f) cooling rate, $r_c = 10$ °C min^{-1}, and heating rate, $r_h = 5$ °C min^{-1}) were used, which were described in details in one of our previous studies [28].

The sub-T_g relaxations were tried to investigate similarly to the T_g. However, the signal of the molecular mobilities at lower temperatures was too small and noisy, and no reproducible results were achieved. For this reason, another experimental setup was tested for determining sub-T_g values (Fig. 2c). During the sample preparation, round pastilles were prepared with a Camilla OL95-type press using 100 bar pressure. The thickness and diameter of the pastilles were ca. 0.5 mm and 12 mm, respectively. Approximately 60 mg of electrospun sample was measured into the press device to reach the 0.5-mm thickness after the pressing. The pressed samples were sized to fit into the copper sample holder of the TSC device, which functioned as the bottom electrode. The upper electrode was the same stainless-steel disk as in the case of T_g determination. Besides, the process parameters were also changed. The T_p was set to well below

the T_g (50 °C, 35 °C, 25 °C, 15 °C, 5 °C, and 0 °C in the case of 0%, 10%, 20%, 30%, 40%, and 50% drug loading, respectively). In this way, the contamination of the electrodes was able to avoid. Besides, the examined sample showed no deformation thus noises originating from the rough surface resulting from volume change disappeared. With this in line, the T_a was also modified to 0 °C in the case of the 40% and 50% samples. For investigating sub-T_g relaxations, T_0 was set to -150 °C, and T_f was 30 °C. In addition, the E was changed to 600 V mm^{-1} to increase the intensity of the depolarization current signal; thus, 300 V polarization voltage (U_p) hit the 0.5-mm sample. All other parameters (t_a, t_p, t_0, r_c, r_h) were not changed.

Raman micro-spectroscopy

For the examination of the molecular segments taking part in relaxation processes, a Horiba Jobin Yvon LabRam system (Horiba France SAS, Longjumeau, France) was applied combined with a Linkam THMS600 heating/cooling stage (Linkam Scientific Instruments Ltd., Salfords, United Kingdom). The laser source was a 785-nm diode laser (~ 3 μm laser spot size), and an Olympus BX-40 optical microscope (Olympus, Tokyo, Japan) was connected to the spectrometer. To improve the resolution, a confocal system was used (100-μm confocal slit and 1000-μm confocal hole). Before reaching the CCD detector, a 950 groove/mm grating monochromator was adapted for dispersing photons by wavelength. The spectrograph position was tuned to the characteristic peaks of the API-s. For NAP samples, it was adjusted to 1150 cm^{-1} to measure the spectral range of 500–1730 cm^{-1}, and for SPIR samples, it was 1200 cm^{-1} to make measurements in a 550–1775 cm^{-1} spectral range. The resolution of substance spectra was 16 cm^{-1} in both cases. The measurements were implemented with a 20 × magnification objective. The used acquisition time was 60 s with 2 as an accumulation number. The applied temperature program contained linear heating between -150 and 150 °C with a heating rate of 2 °C min^{-1}. Pastilles were formed with approximately 18–20 mg of electrospun sample to eliminate the negative effect of laser light scattering. Manual compression was used to produce the flat-surfaced pastilles with a thickness of around 0.5 mm. The compression was executed in copper TSDC sample holders surrounded by a Teflon ring. The recorded Raman spectra were evaluated in LabSpec 5.41 (Horiba Jobin Yvon S.A.S., Villeneuve d'Ascq, France). As the preparation of the spectra, smoothing, baseline correction, and normalization were used and peak fitting was performed for the peaks showing significant changes. The information obtained from the evaluation
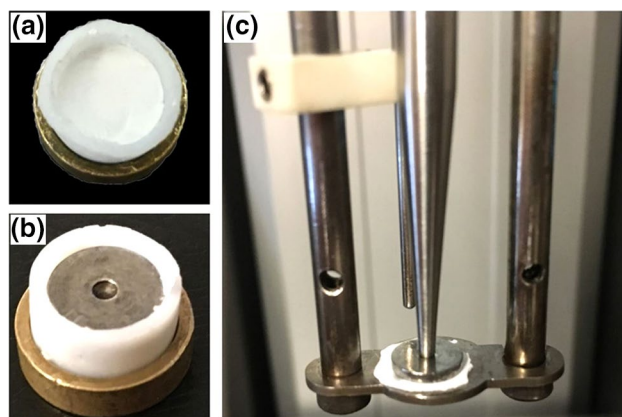

Fig. 2 Photos of the TSDC measuring setup. The measured sample after compression (a); measuring cell for T_g determination (b); sample and upper electrode inlayed into the TSCII device for sub-T_g measurements (c)
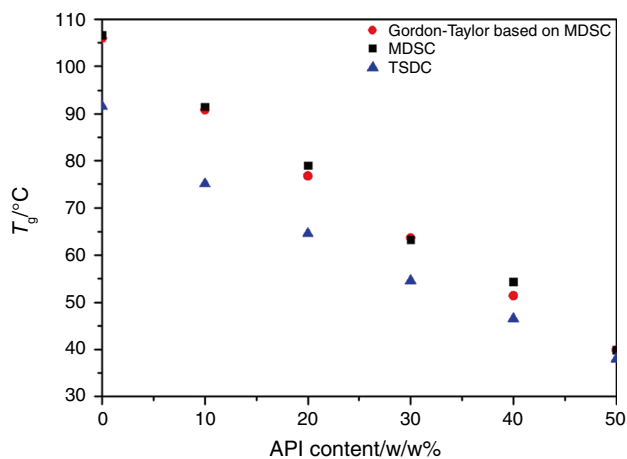
Fig. 3 Measured and calculated T_g values of NAP-loaded samples [28]

Table 1 Measured and calculated T_g values of NAP-loaded samples as shown in Fig. 3

NAP content/%	T_g by Gordon–Taylor equation/°C	T_g by MDSC/°C	T_g by TSDC/°C
0	106	107	92
10	91	92	75
20	77	79	65
30	64	63	55
40	51	54	47
50	40	40	38

was full width at half maximum (FWHM), Raman shift, Raman intensity, and area under the curve. The values were plotted as a function of temperature.

Results and discussion

Comparison of T_g changes of the 'strongly interacting' and 'less interacting' ASDs

In one of our previous studies, the T_g of the NAP-loaded samples containing 10, 20, 30, 40, and 50% API was already investigated with both MDSC and TSDC (Fig. 3, Table 1) [28]. According to those MDSC results, a slight increase in the T_g was observed from 20% drug loading compared to the T_g calculated by the Gordon–Taylor equation (Eq. 1). The results suggested that intermolecular interactions can form between the API and the polymer above 20% drug content as the positive deviation from the theoretically calculated values refers to strong molecular forces [35]. In addition, the tendency of the T_g values was similar in the case of the TSDC measurements. The greater variation from the calculated values and T_g-s measured by TSDC can be explained with that the T_g of the pure component used in the Gordon–Taylor equation was determined by MDSC.

As the changes in the T_g values of 'strongly interacting' drug-polymer systems were known from our previous study, the analysis of the T_g of 'less interacting' ASDs was in the focus of the present work. Both MDSC and TSDC results of SPIR-loaded samples showed single T_g suggesting molecularly dispersed ASDs. Besides, the plasticization effect of the API was also visible as the increasing SPIR content led to decreased T_g values, similarly to the case of the NAP-loaded samples (Fig. 4, Table 2). It means from another point of view that the polymer has an 'antiplasticization' effect on the
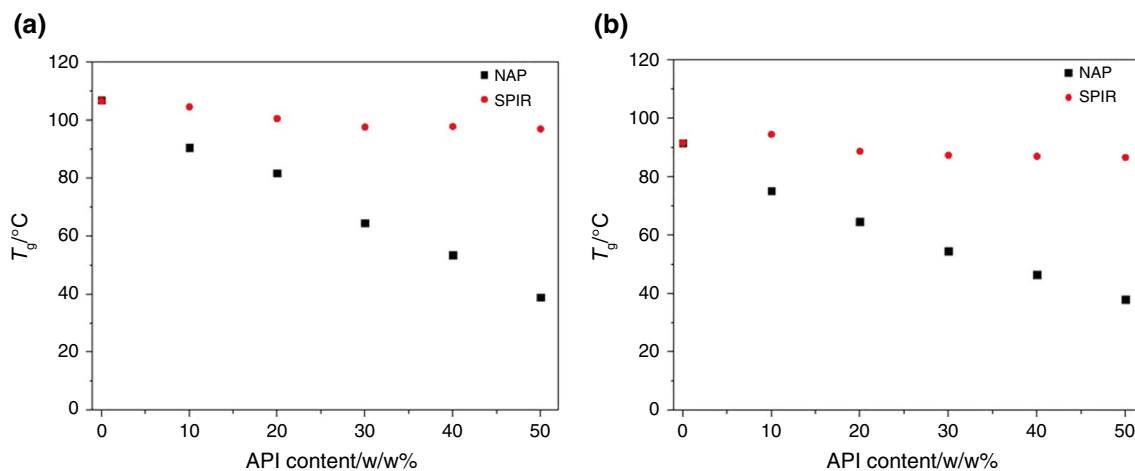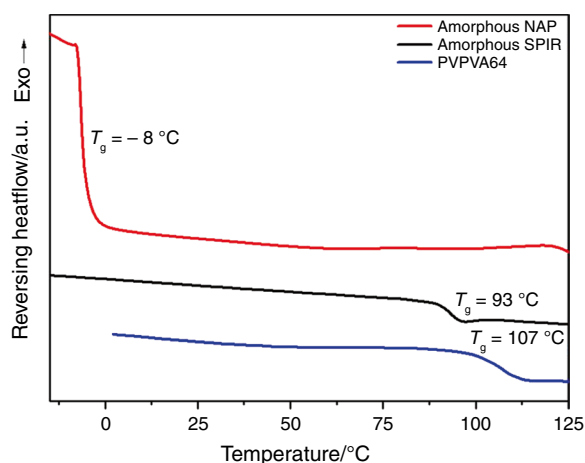

Fig. 4 T_g values of the different compositions measured by MDSC (**a**) and TSDC (**b**) methods

**Table 2** T_g values of the different compositions measured by MDSC **a** and TSDC **b** as shown in Fig. 4

MDSC/%	NAP T_g/°C	SPIR T_g/°C
0	107	107
10	91	105
20	82	101
30	64	98
40	53	98
50	39	97
TSDC/%	NAP T_g/°C	SPIR T_g/°C
0	92	92
10	75	95
20	65	89
30	55	87
40	47	87
50	38	87

amorphous APIs [36]. However, the tendency was less visible in the case of the SPIR-loaded ASDs. For better understanding, theoretical calculations were also performed for the samples containing SPIR.

To calculate the theoretical T_g values of SPIR-loaded samples with the Gordon–Taylor equation (see in the 'Materials and methods' section), the T_g-s of the pure components were determined by MDSC (Fig. 5). The measured T_g of the amorphous SPIR was closer to the T_g of the PVPVA64 than in the case of the NAP [28], which explains that the T_g of SPIR-loaded ASDs also varies within a narrower range. The determined T_g values of the pure component were similar to other publications (despite the different parameters of the amorphization or the MDSC measurement) [12, 37]. The densities of the pure components, that is also needed for the calculations of the Gordon–Taylor equation, were taken from references [37] and [38].

Comparison of the T_g-s of the SPIR-loaded samples determined by MDSC, TSDC, and theoretical calculation is summarized in Fig. 6 and Table 3. The T_g-s measured by MDSC were a bit lower than that of the calculated values.
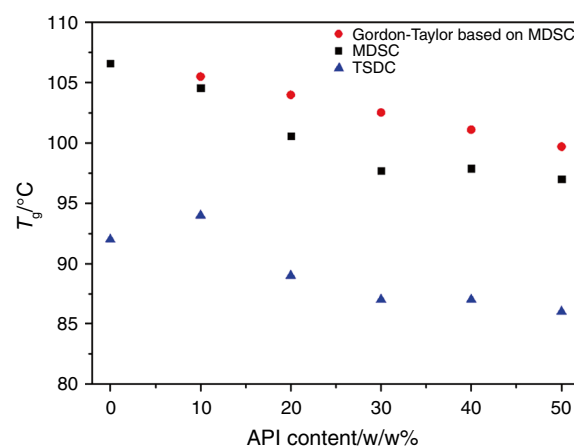
Fig. 6 The measured and calculated T_g values of SPIR-loaded samples

Table 3 The measured and calculated T_g values of SPIR-loaded samples as shown in Fig. 6

SPIR content/%	T_g by Gordon–Taylor equation/°C	T_g by MDSC/°C	T_g by TSDC/°C
0	–	107	92
10	105	105	94
20	104	101	89
30	103	98	87
40	101	98	87
50	100	97	86

Fig. 5 Reversing heat flow of the pure NAP, SPIR, and PVPVA64 samples in the function of the temperature

The negative deviation from the T_g-s calculated by the Gordon–Taylor equations indicates that the interactions between the drug and the polymer are weaker than interactions within the individual components [35]. Although the calculations are based on MDSC data and the principle of TSDC measurement is different, the observed T_g trends were similar, aligning with the theory according to which deviations from the T_g calculated by the Gordon–Taylor equation depend on the intermolecular interaction. Strong drug-polymer interactions, like H-bonding in the case of NAP-PVPVA systems, lead to positive deviations between the measured and the calculated values. In contrast, the absence of strong intermolecular interactions, such as lack of H-bond between the API and the polymer as seen in SPIR-PVPVA64 systems, results in negative deviation compared to the calculated data. Furthermore, the results of the present research highlight that the API-loading affects the deviation between the measured and theoretical T_g values. As the intramolecular and intermolecular interactions can influence the stability and the dissolution of the ASDs, it could be useful to search for a correlation between these findings and the stability in a future work. In addition, a special ASD preparation method, the electrospinning was used during our experiments, which can also influence the changes of the T_g. Therefore, it could be interesting in a next study to compare the physical behavior of 'strongly interacting' and 'less interacting', which are prepared by different techniques.

Examination of the sub-T_g relaxations by TSDC measurements

To investigate the sub-T_g relaxations of 'strongly interacting' and 'less interacting' or possibly 'non-interacting' ASDs, TSDC measurements were performed as small molecular motions can be detected with this method [39].

The obtained results are illustrated in Fig. 7. Although the sample thickness and the fiber morphology influenced the intensity and width of the TSDC curves, all depolarization current curves show a peak around -130 °C that indicates the β-relaxation of the ASDs. The sub-T_g values were determined as the temperature corresponding to the peak maximum.

Based on the results, a clear correlation can be found between the sub-T_g and the NAP content (Fig. 8). By increasing API content in the 'strongly interacting' system, the sub-T_g is increasing as well. However, it means that the sub-T_g changes in an opposite way compared to the T_g with increasing drug loading. According to the results of Thayumanasundaram et al. [27], a similar phenomenon was observed in the case of indomethacin and PVPVA64 spray-dried samples. The shift in the sub-T_g values can be explained by the H-bond interactions between the API and the polymer. Below the glass transition (α-relaxation), the
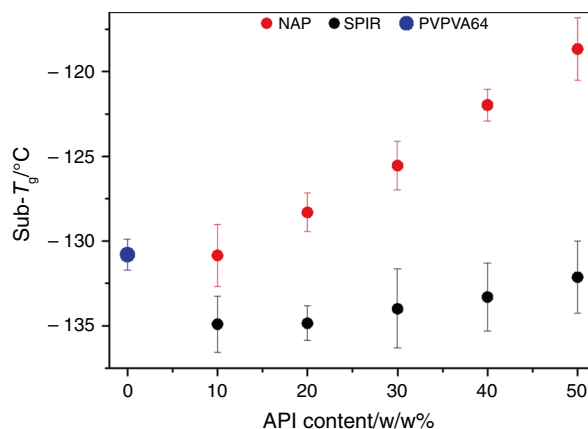

Fig. 8 Sub-T_g values of the NAP-loaded and SPIR-loaded samples based on the TSDC measurement
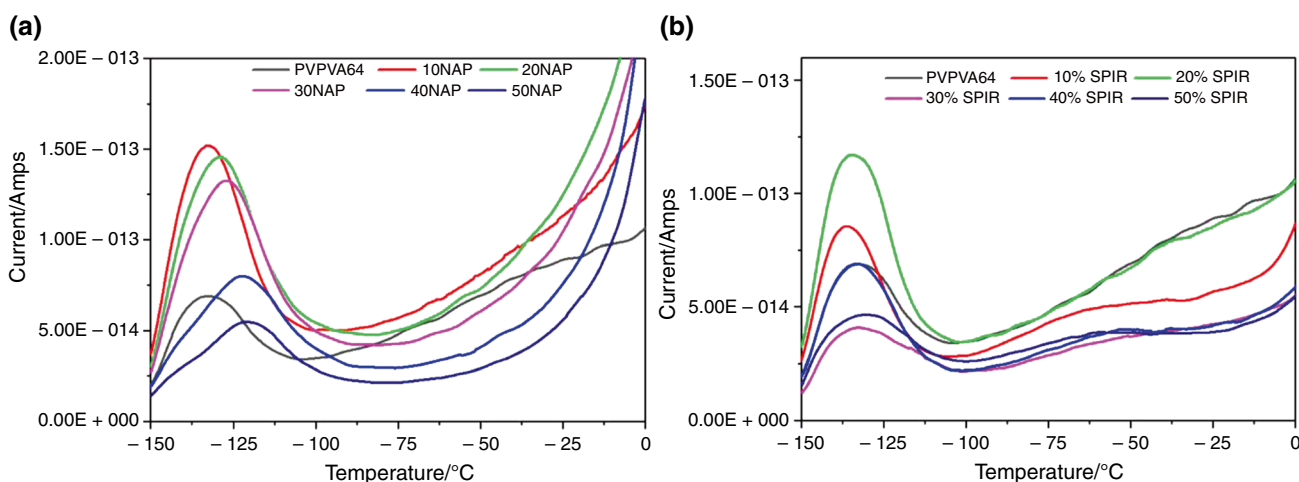

Fig. 7 TSDC curves of the NAP-loaded (**a**) and SPIR-loaded (**b**) samples

ASD system is characterized by molecular mobility, which corresponds to the side groups or the movement of a smaller number of carbon atoms (not to the movement of the segments). If the ASD contains a smaller amount of H-bond donor molecule (in this case NAP molecule), then fewer groups participate in the intermolecular H-bond interaction and the remaining 'free' groups can move easily. In this way, sub-T_g relaxations can start at lower temperatures in the case of lower API content. With the increasing amount of H-bond donor molecule (NAP with hydroxyl group), more groups of the polymer can take part in the intermolecular H-bond interaction, and more H-bond can form resulting in a stronger 'interacting' system. Therefore, a higher temperature is needed to initiate molecular motions (sub-T_g relaxations).

In contrast, the sub-T_g of SPIR-loaded ASDs decreased slightly compared to the pure polymer. The lower sub-T_g values suggest that there is no interaction between the API and the polymer, what is more, the presence of the API inhibits the polymer–polymer interactions. Therefore, the molecular mobility will increase, and sub-T_g transition can occur at lower temperatures. The small increase of sub-T_g in the function of SPIR content suggests segregations within the ASDs, possibly indicating the onset of nanoscale phase separations in these systems. However, the sub-T_g changes were quite small; thus, investigation of other 'less interacting' or 'non-interacting' ASDs might be useful in the future to confirm this assumption.

Investigation of the relaxations' molecular background by Raman spectroscopy

Examination of the glass transition

The MDSC and the TSDC results showed that the T_g and sub-T_g values are influenced by the API content, especially in the case of the 'strongly interacting' systems. However, it is unknown, which part of the molecules affects the different relaxations exactly. To investigate the molecular background of the relaxations, measurements were made with Raman spectroscopy in the function of temperature since this vibrational spectroscopic method is suitable for examining different bond environments.

In-depth examination of T_g by Raman spectroscopy proved to be quite challenging in the case of the prepared drug-loaded ASDs. Due to the temperature rise, the samples turned to be transparent and showed a glassy structure. For this reason, the autofocus mode of the equipment was not able to find the correct position in all cases resulting in wrong signal, for example in the case of 10% NAP loading (Fig. 9a). However, the temperature at which the last clear and intensive spectrum was measured (at 94 °C) is almost the same as the T_g measured by MDSC (92 °C). With increasing API content, the change of the sample became less intense, allowing for the recording of appropriate spectra through the autofocus mode. In spite of this, a decrease in the intensity was observed from 74 °C, which temperature was above the T_g measured by MDSC (63 °C). After few measuring points, the autofocus was able to follow the changes in the sample, and spectra with higher intensities were recorded again (Fig. 9b).

Similar observations were made in the case of SPIR-loaded samples that the intensity of the Raman spectra decreased above the T_g determined by MDSC (Fig. 10). In addition, the ASDs containing SPIR also became transparent above the T_g suggesting that the API and the polymer form a miscible system [40], which explains the single T_g measured by MDSC and TSDC. This assumes that even if there is no interaction between SPIR and PVPVA64, dissolving the components in the solvents resulted in a molecularly dispersed solution, which remained as amorphous solid solution after the extremely quick solvent evaporation during the electrospinning.

Although Raman spectroscopy coupled with the Linkam heating/cooling stage did not allow as precise determination of the T_g as the MDSC, the changes in the intensity and temporary loss of focus indicated well the glass transition during the Raman measurements. It confirmed that the segment movement started at those temperatures.

Investigation of the sub-T_g transitions in the case of the polymer and the 10% NAP-loaded sample

In contrast with the glass transition, no change was observed in the macroscopic structure of the samples at lower temperatures suggesting a better chance to investigate the molecular background of the sub-T_g relaxations measured by TSDC.

During the evaluation of the spectra below the T_g, the data range was reduced at first to avoid the noise from the wrong spectra around the T_g. Then, preprocessing steps (smoothing, baseline correction, and normalization) were performed for all spectra (Fig. 11a). In the next phase of data analysis, the spectrum recorded at the starting temperature (at − 150 °C) was subtracted from all the other spectra to explore the Raman bands, which changed in the function of the temperature (Fig. 11b). After that, only the peaks, that showed significant change, were evaluated by peak fitting (Fig. 11c). In this way, the Raman shift, the Raman intensity, the full width at half maximum (FWHM), and the area under the curve were determined and depicted in the function of temperature.

Comparing the results after the subtraction in the case of the polymer and the sample containing 10%NAP, similarities can be seen (Fig. 12). Characteristic Raman bands of PVPVA64 are also noticeable during the evaluation of 10% NAP-loaded sample.
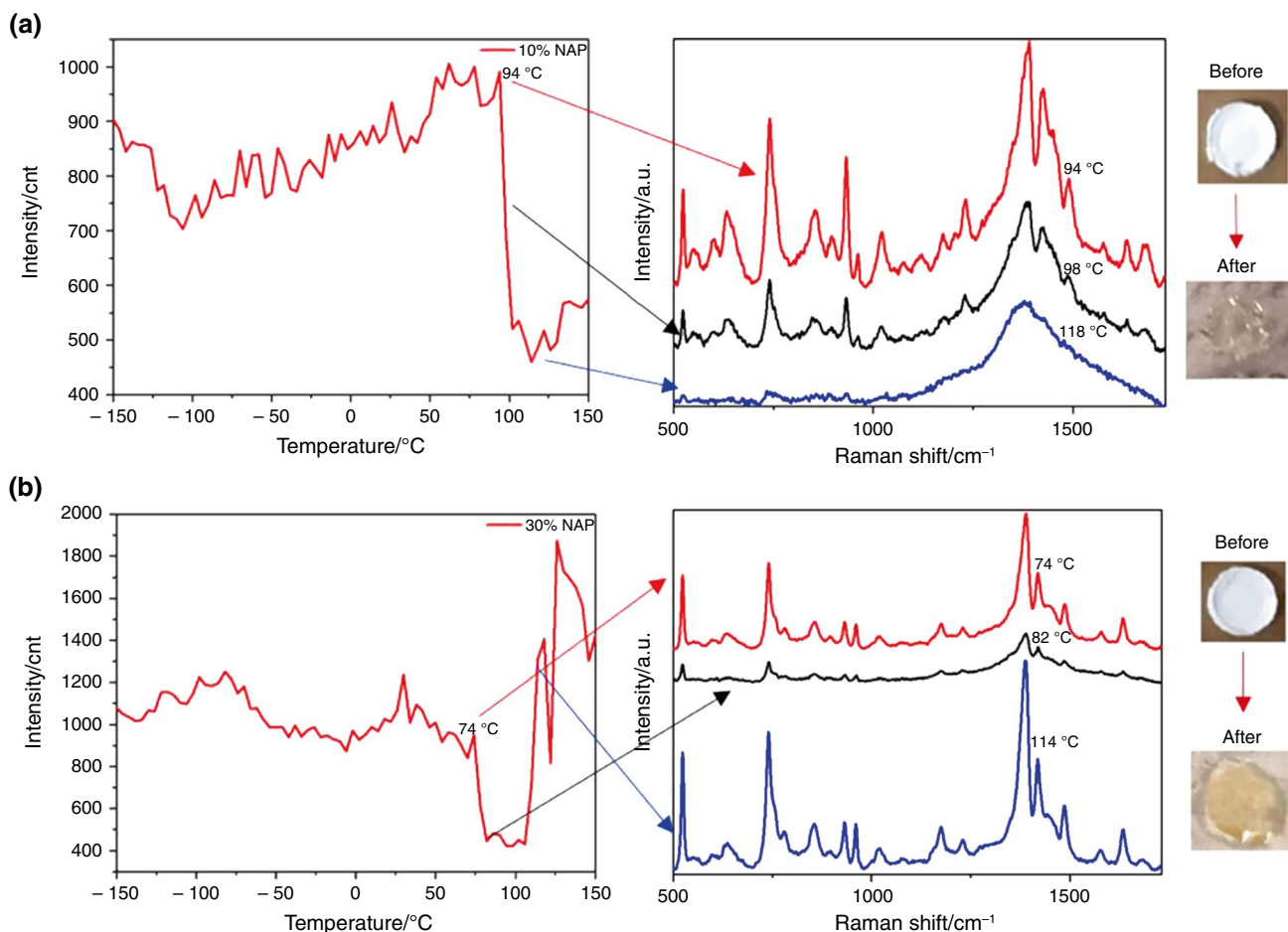
(a)

(b)

Fig. 9 Changes of the intensity of Raman spectra in the function of temperature by 10% (**a**) and 30% (**b**) NAP-loaded samples. Photos illustrate the changes in the samples' structure before and after the measurements (right side of the Figure)

Two peaks, at 744 cm^{-1} and 933 cm^{-1}, are especially interesting as showing the most evident changes in the function of temperature. Both peaks are associated with the pyrrolidone ring. The peak around 743–744 cm^{-1} relates to the C–C stretching in the pyrrolidone part of the PVPVA64 while the peak around 933 cm^{-1} corresponds to the C–C ring breathing [41, 42]. The prominence of these peaks suggests that at low API content, the polymer, more precisely the pyrrolidone ring of the PVPVA64, determines the sub-T_g relaxation. After the peak fitting, the Raman intensity and the peak area showed maxima in the function of temperature at −122 °C (Fig. 13), indicating the sub-T_g transition of the polymer.

Investigating the changes of these peaks in the 10% NAP-loaded sample, a maximum of peak intensity and peak area is visible in the function of temperature at around -130 °C suggesting that the pyrrolidone ring has a sub-T_g relaxation at this temperature range (Fig. 14). The sub-T_g values determined from the Raman spectroscopic measurements are close to the results of the TSDC method. Therefore, the

temperature-dependent Raman experiments proved to be suitable for detecting sub-T_g transitions in the case of the 10%NAP-loaded ASD. The slight differences between the results of the peaks at 744 cm^{-1} and 933 cm^{-1} suggest that Raman spectroscopy enables us to distinguish the steps and molecular background of the sub-T_g transitions.

Investigation of the sub-T_g transitions in the case of higher NAP-loaded samples

With increasing API-loading, evident changes can be seen at 522–524 cm^{-1}, 741–743 cm^{-1}, and 1391–1393 cm^{-1} (Fig. 15), which are all associated to the naphthalene ring of the NAP [43–45].

The peak at 522–524 cm^{-1} corresponds to the in-plane ring deformation [43], the peak at 741–743 cm^{-1} is related to the ring vibration, and the peak at 1391–1393 cm^{-1} is associated to C-H ring bending and C–C ring stretching [45]. As the change of the peak at 524 cm^{-1} was less than that of the other two highlighted peaks, only the latter two
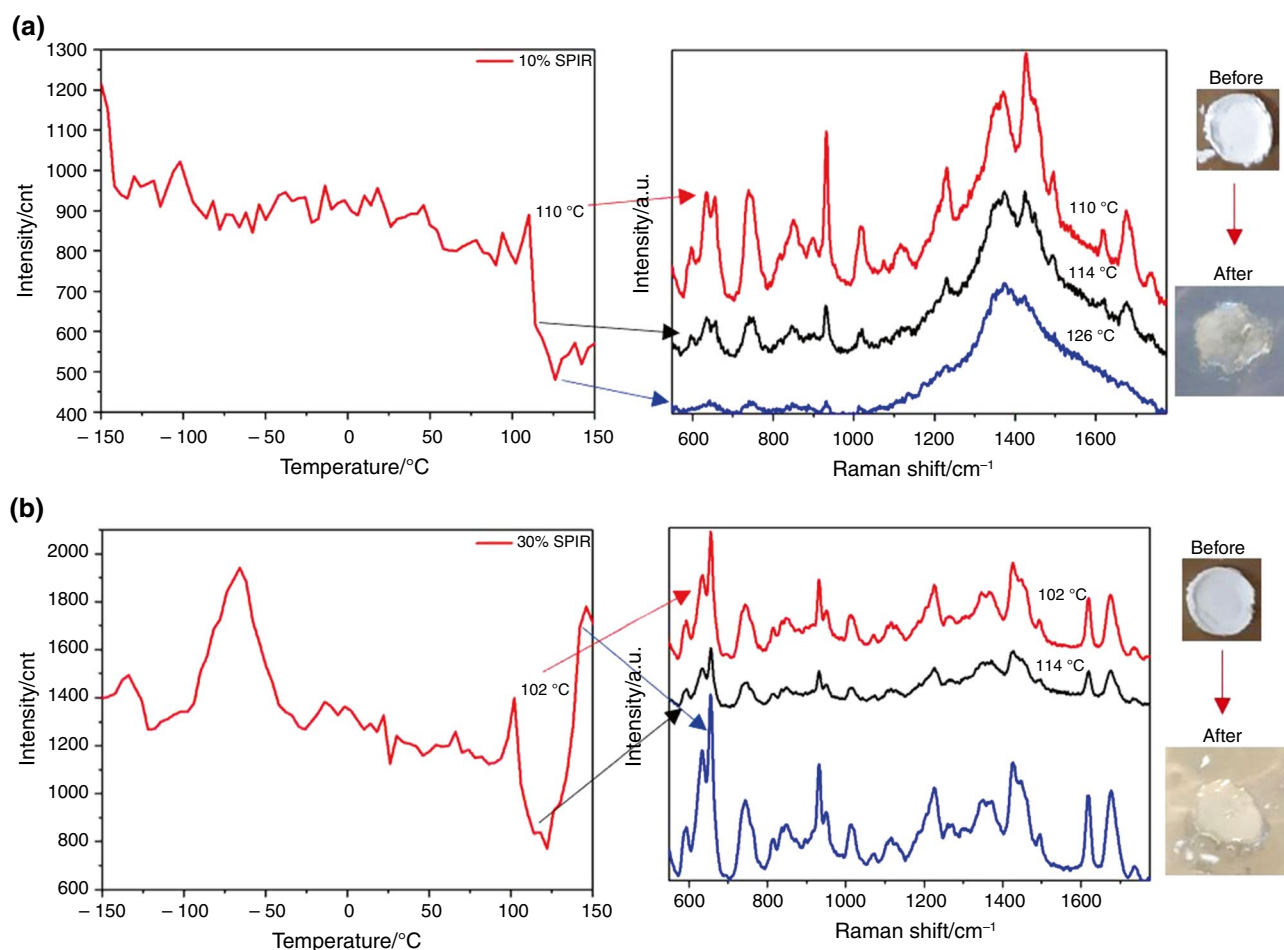
Fig. 10 Changes of the intensity of Raman spectra in the function of temperature by 10% (**a**) and 30% (**b**) SPIR-loaded samples. Photos illustrate the changes in the samples' structure before and after the measurements (right side of the Figure)

were evaluated in-depth. Depiction of the key parameters in the function of temperature showed interesting tendencies (Figs. 16 and 17). The Raman intensity of the peak at 741–743 cm^{-1} reached a maximum at different temperatures in the case of the 30%, 40%, and 50% NAP-loaded samples (Fig. 16). The place of the maximum might indicate those temperatures, where the sub-T_g transitions occur [32]. Although these temperature values differ from the sub-T_g values measured by TSDC, some of the maxima are close to those temperatures. The multiple sub-T_g values by temperature-dependent Raman measurements assume that sub-T_g relaxations take place in more steps, which is a characteristic feature of small molecules. Considering the peak intensity in the function of temperature, similar maximums were visible in the case of the peak at 1388–1392 cm^{-1} (Fig. 17). However, a peak shift was also visible in this region. With an increasing API content, the peak in question was characterized by a higher Raman shift, which can be explained by the intermolecular interaction between the NAP and the PVPVA64. In addition, the Raman shift decreased in the

function of temperature indicating the temperature-dependent volume expansion of the ASDs [33]. The outstanding changes of these investigated peaks versus temperature suggest that the aromatic ring of NAP influences significantly the sub-T_g relaxations at higher drug loading in the 'strongly interacting' system; thus, it can be a crucial part of ASD with regard to the stability.

Examination of the sub-T_g transitions of SPIR-loaded samples

In contrast with the NAP-loaded samples, subtracting results of the ASDs containing SPIR did not show clear outstanding peaks (Fig. 18). The graph of the 10% SPIR-loaded sample was similar to the subtraction results of the pure PVPVA64 while with increasing API content, the changes of the characteristic peak of the polymer decreased. However, no evident changes were observed in the case of the 'less interacting' system indicating the lack of interaction between the SPIR and the PVPVA64.
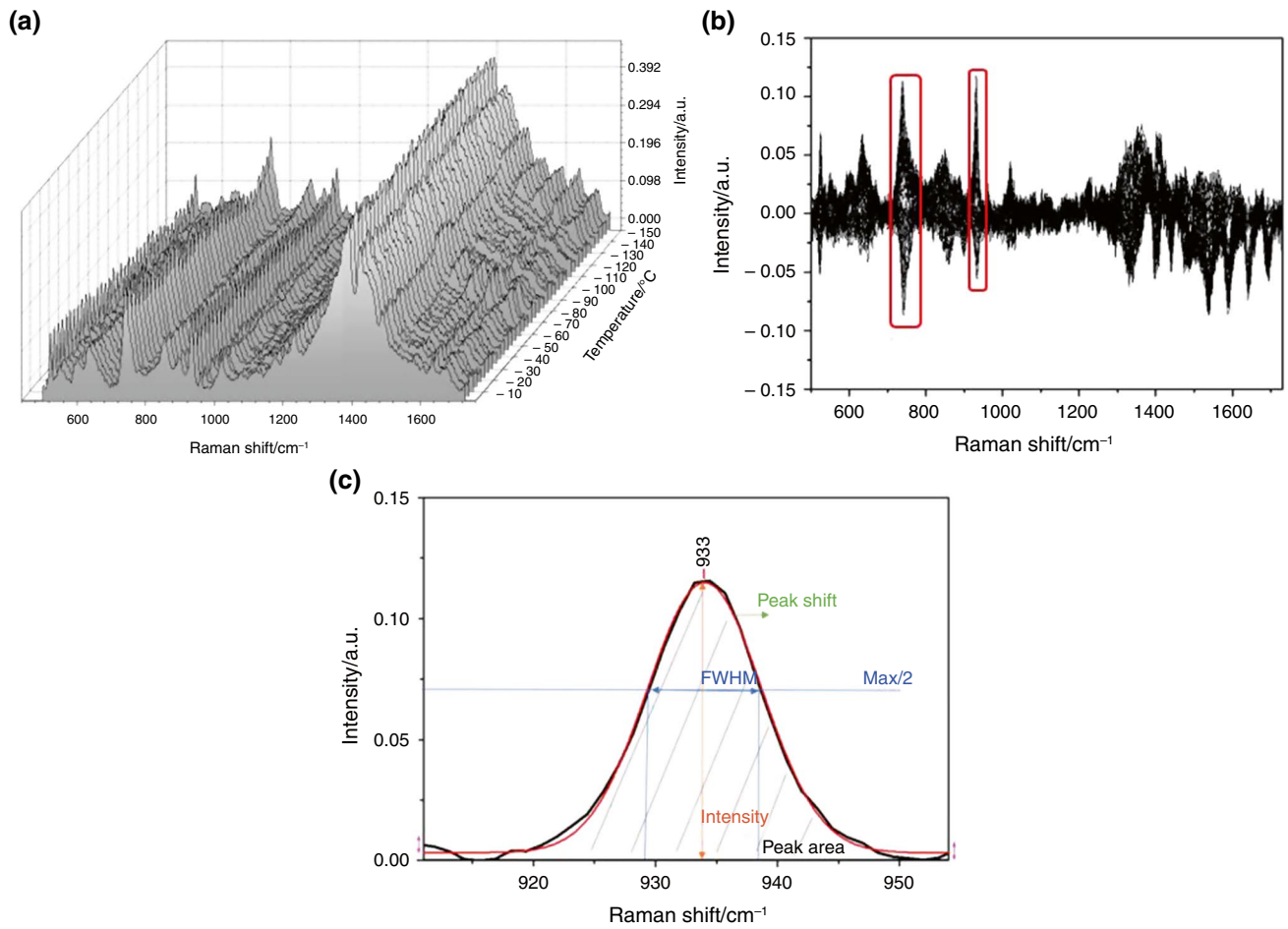
(a)

(b)

(c)

Fig. 11 Pre-processed Raman spectra (**a**), the spectra after subtraction of the spectrum obtained at the starting temperature (**b**), and the peak fitting in the case of the 10% NAP-loaded sample (**c**)
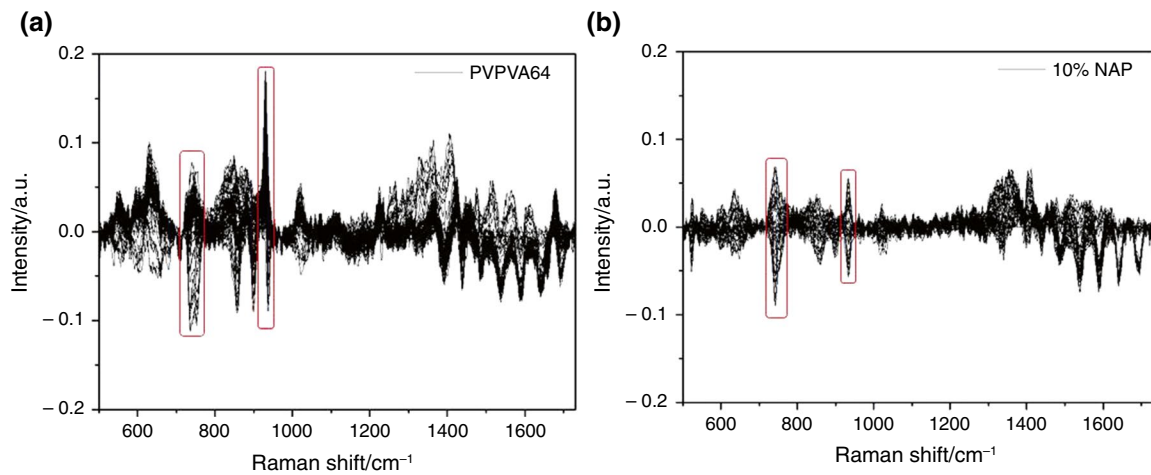
(a)

(b)

Fig. 12 Subtraction results of the spectra recorded in the function of temperature in the case of PVPVA64 (**a**) and 10% NAP-loaded ASD (**b**)
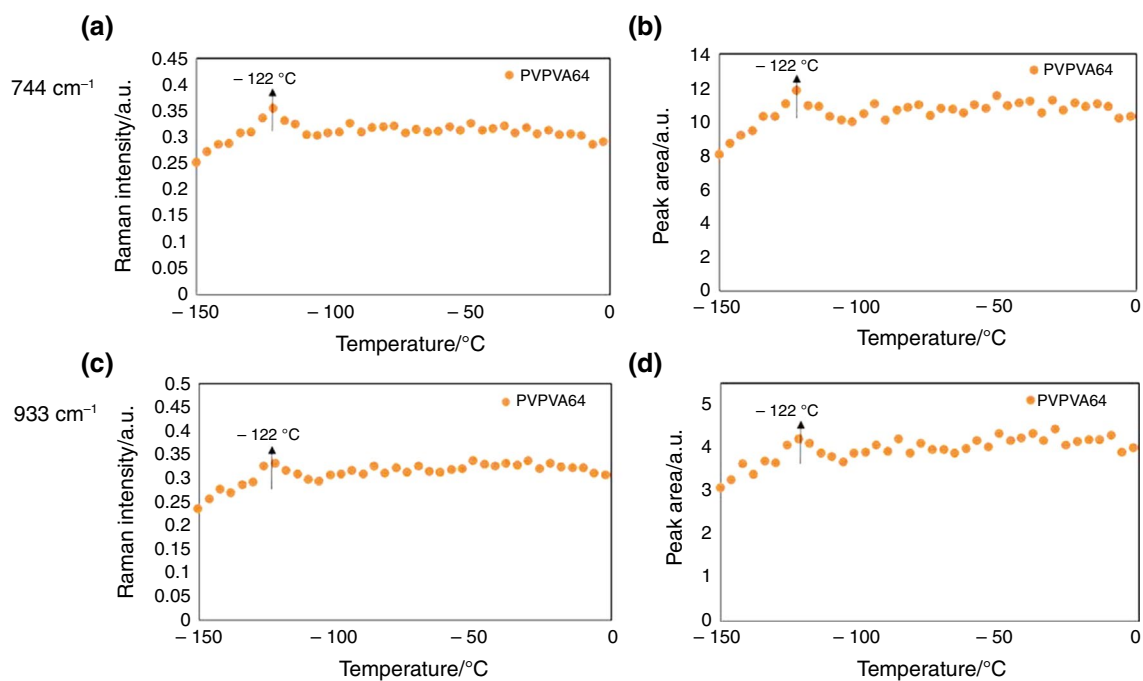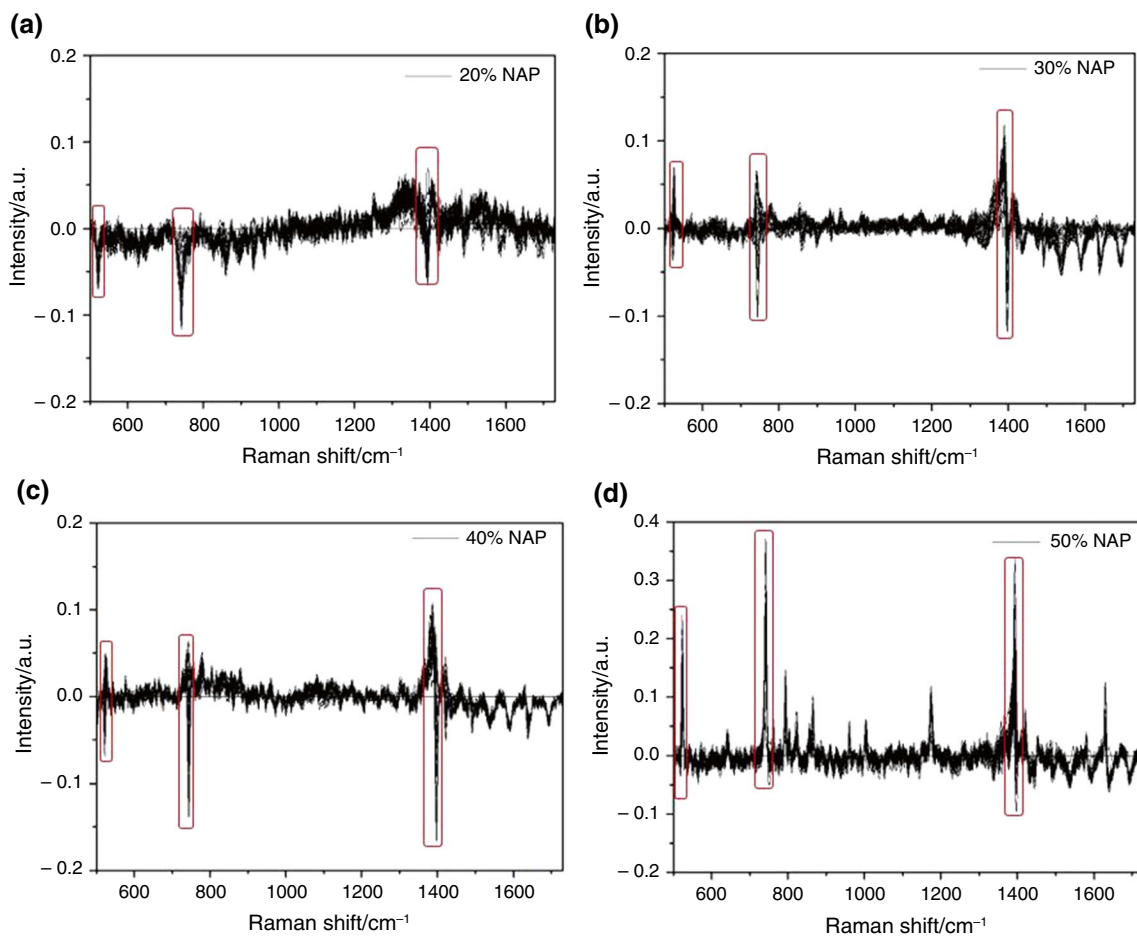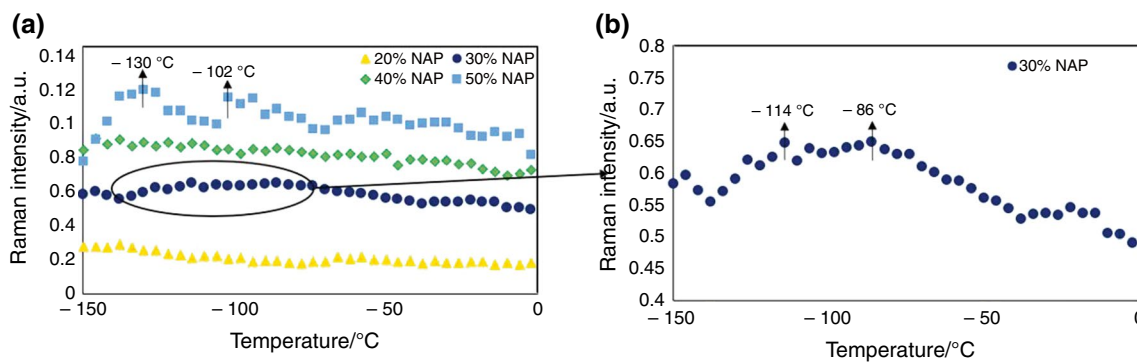
Fig. 13 Temperature dependence of Raman intensity (**a**) and peak area (**b**) at the 744 cm^{-1} peak, and temperature dependence of Raman intensity (**c**) and peak area (**d**) at the 933 cm^{-1} peak in the case of the polymer
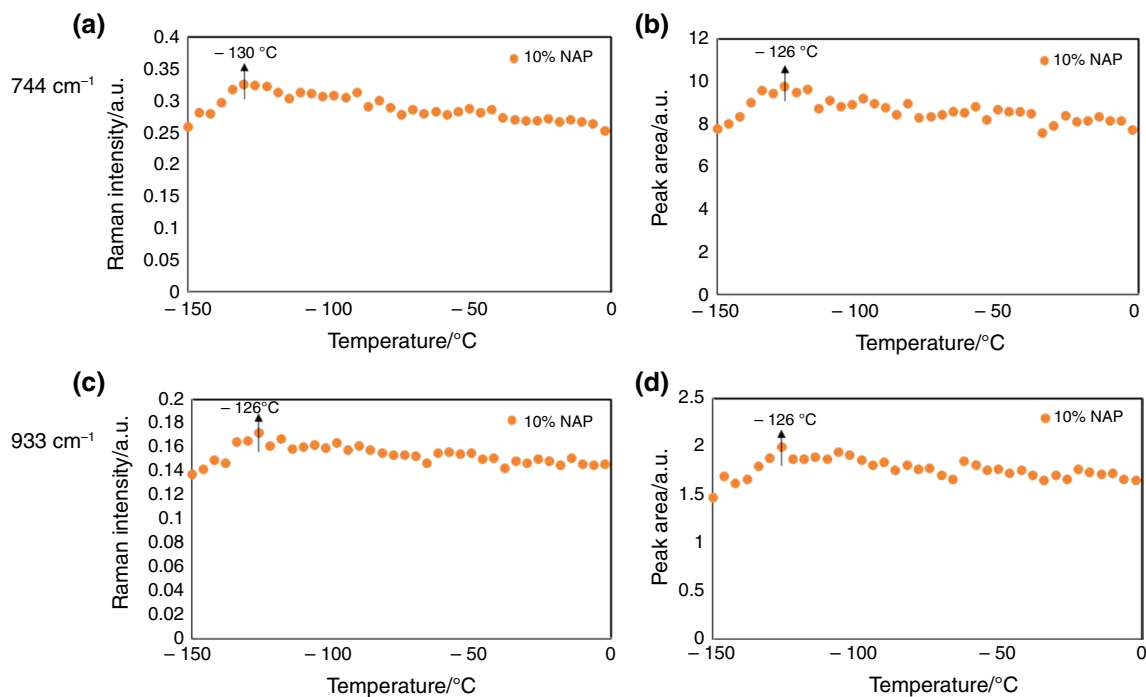
Fig. 14 Temperature dependence of Raman intensity (**a**) and peak area (**b**) at the 744 cm^{-1} peak, and temperature dependence of Raman intensity (**c**) and peak area (**d**) at the 933 cm^{-1} peak in the case of 10% NAP-loaded sample

Fig. 15 Subtraction results of the spectra recorded in the function of temperature in the case of 20% (**a**), 30% (**b**), 40% (**c**), and 50% (**d**) NAP-loaded ASDs

Fig. 16 Temperature dependence of Raman intensity in the case of 20%, 30%, 40%, and 50% NAP-loaded ASDs at the peak around 743 cm.$^{-1}$ (**a**) and highlighting the curve of 30% NAP-loaded ASD (**b**)
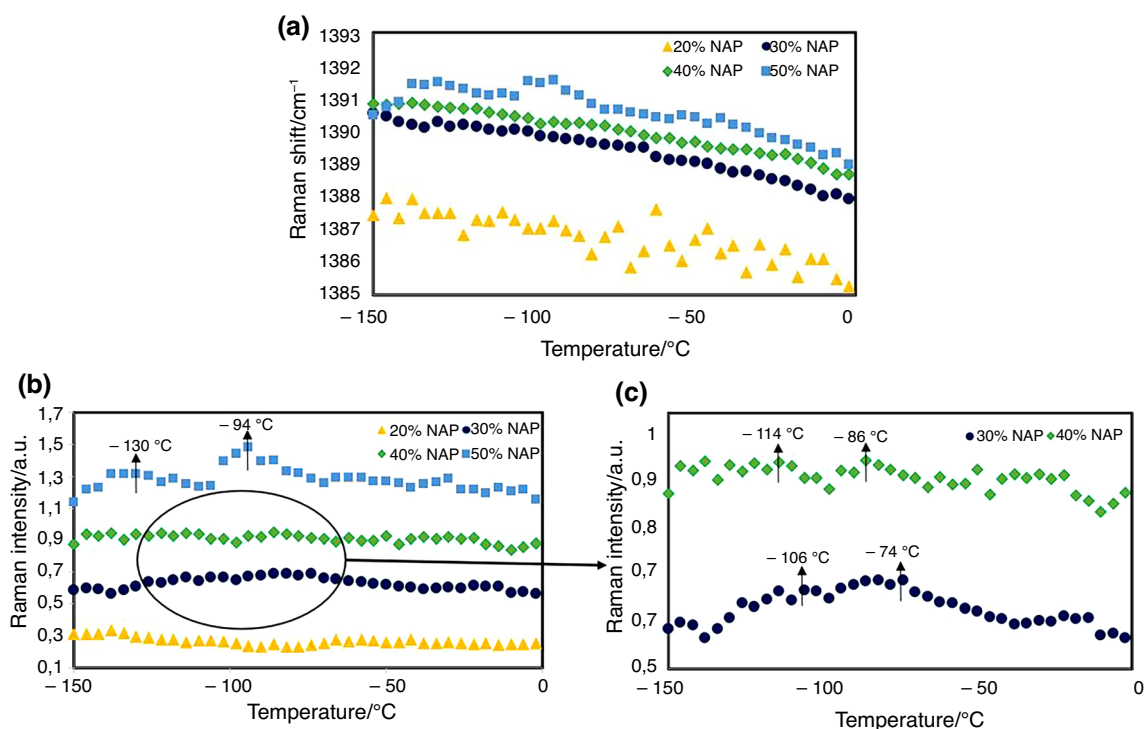
Fig. 17 Temperature dependence of Raman shift (**a**) and Raman intensity (**b**) in the case of 20%, 30%, 40%, and 50% NAP-loaded ASDs at the peak between 1386 and 1392 cm.$^{-1}$, and highlighting the curves of 30% and 40% NAP-loaded samples (**c**)
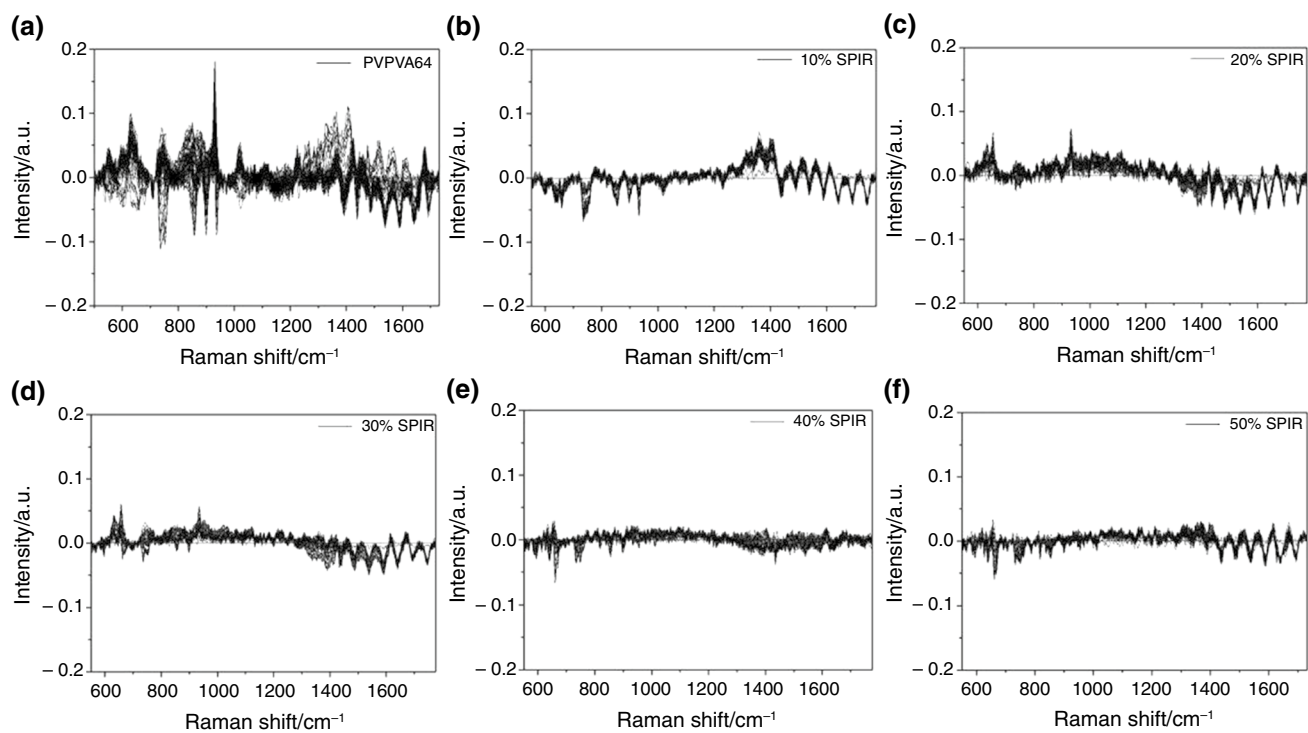
Fig. 18 Subtraction results of the spectra recorded in the function of temperature in the case of PVPVA64 (**a**), 10% (**b**), 20% (**c**), 30% (**d**), 40% (**e**), and 50% (**f**) SPIR-loaded ASDs

The Raman spectra recorded at different temperatures confirmed the TSDC results and proved that the SPIR-PVPVA64 system is a 'non-interacting' ASD. While the characteristic peaks of NAP have changed in the function of temperature in the sub-T_g region, the characteristic peak of the SPIR did not show changes, suggesting that the relaxation of the polymer dominates in the ASDs containing SPIR and PVPVA64.

Conclusions

In this study, a comprehensive thermal analysis of the relaxations was performed in the case of an 'interacting' and a 'non-interacting' ASD system. The plasticization effect of the APIs was visible based on the measured T_g values of the ASDs containing NAP or SPIR. The decrease of the T_g in the function of API content was significantly larger in the case of NAP-loaded samples, which can be explained by the lower T_g of the pure amorphous API. From this context, preparation of ASDs with increased NAP content is not recommended as instability issues can occur more easily at the storage temperature. However, it is worth noting that T_g is not the only property of ASDs that can influence stability. Different intramolecular or intermolecular interactions or sub-T_g relaxations may also affect the stability, and thus, the applicability of the ASDs in final dosage forms. The comparison of the measured T_g values with the theoretical values assumed that intermolecular interactions can form between NAP and PVPVA64 as the measured results showed positive deviation from the calculated ones. In contrast, negative deviation was observed in the case of SPIR-loaded samples suggesting no intermolecular interaction between the API and the polymer. In terms of sub-T_g relaxations, TSDC results also confirmed the possibility of intermolecular H-bond interaction between the polymer and the NAP as the opposite tendency was observed compared to the T_g values. Considering that the sub-T_g relaxations are related to molecular movements, the 'free'/'less interacting' parts of the molecules can be relaxed at lower temperatures. In other words, it means that in the case of 'interacting' systems, the increasing amount of H-bond donor molecule (in this case NAP) can make difficult the molecular movements resulting in higher sub-T_g values. Furthermore, TSDC results assumed the lack of intermolecular interactions in the case of ASDs containing SPIR and PVPVA because the sub-T_g decreased compared to the pure polymer.

The temperature-dependent Raman experiments strengthened the results of the TSDC measurements as the peak of the NAP relating to the C-H ring bending and C–C ring stretching showed a shift in the function of API content suggesting the intermolecular interactions in the ASD. In addition, the depiction of intensity and peak area of NAP-loaded samples in the function of temperature showed maximum values at different temperatures indicating the sub-T_g relaxations of the systems. In contrast, no changes were observed in the SPIR-loaded samples, which proved the 'non-interacting' behavior of ASDs containing SPIR and PVPVA64.

The results highlighted that the simultaneous application of different methods, such as DSC and Raman spectroscopy or TSDC and Raman spectroscopy, can open up new ways in the understanding of relaxations of ASDs. Thereby, the stability of the amorphous pharmaceuticals can become more consciously planned, which greatly helps the early stages of development.

Declarations

References

1. Pandi P, Bulusu R, Kommineni N, Khan W, Singh M. Amorphous solid dispersions: an update for preparation, characterization,

mechanism on bioavailability, stability, regulatory considerations and marketed products. Int J Pharm. 2020;586: 119560. https://doi.org/10.1016/j.ijpharm.2020.119560.

2. Liu X, Feng X, Williams RO, Zhang F. Characterization of amorphous solid dispersions. J Pharm Investig. 2018;48:19–41. https://doi.org/10.1007/s40005-017-0361-5.

3. Rahman Z, Siddiqui A, Gupta A, Khan M. Regulatory considerations in development of amorphous solid dispersions. In: Shah N, Sandhu H, Choi D, Chokshi H, Malick A, editors. Amorphous solid dispersions: theory and practice. Springer; 2014. p. 545–63. https://doi.org/10.1007/978-1-4939-1598-9_17

4. Guo Y, Shalaev E, Smith S. Physical stability of pharmaceutical formulations : solid-state characterization of amorphous dispersions. Trends Anal Chem. 2013;49:137–44. https://doi.org/10.1016/j.trac.2013.06.002.

5. Lehmkemper K, Kyeremateng SO, Heinzerling O, Degenhardt M, Sadowski G. Long-term physical stability of PVP- and PVPVA-amorphous solid dispersions. Mol Pharm. 2017;14:157–71. https://doi.org/10.1021/acs.molpharmaceut.6b00763.

6. Li R, Lin D, Roos YH, Miao S. Glass transition, structural relaxation and stability of spray-dried amorphous food solids: a review. Dry Technol. 2019. https://doi.org/10.1080/07373937.2018.1459680.

7. Bhugra C, Pikal MJ. Role of thermodynamic, molecular, and kinetic factors in crystallization from the amorphous state. J Pharm Sci. 2008;97:1329–49. https://doi.org/10.1002/jps.21138.

8. Johari GP, Kim S, Shanker RM. Dielectric relaxation and crystallization of ultraviscous melt and glassy states of aspirin, ibuprofen, progesterone, and quinidine. J Pharm Sci. 2007;96:1159–75. https://doi.org/10.1002/jps.20921.

9. Gupta P, Kakumanu VK, Bansal AK. Stability and solubility of celecoxib-PVP amorphous dispersions: a molecular perspective. Pharm Res. 2004;21:1762–9. https://doi.org/10.1023/B:PHAM.0000045226.42859.b8.

10. Teja SB, Patil SP, Shete G, Patel S, Bansal AK. Drug-excipient behavior in polymeric amorphous solid dispersions. J Excip Food Chem. 2013;4:70–94.

11. Dedroog S, Huygens C, Van den Mooter G. Chemically identical but physically different: a comparison of spray drying, hot melt extrusion and cryo-milling for the formulation of high drug loaded amorphous solid dispersions of naproxen. Eur J Pharm Biopharm. 2019;135:1–12. https://doi.org/10.1016/j.ejpb.2018.12.002.

12. Alhalaweh A, Alzghoul A, Mahlin D, Bergström CAS. Physical stability of drugs after storage above and below the glass transition temperature: relationship to glass-forming ability. Int J Pharm. 2015;495:312–7. https://doi.org/10.1016/j.ijpharm.2015.08.101.

13. Thakkar R, Thakkar R, Pillai A, Ashour EA, Repka MA. Systematic screening of pharmaceutical polymers for hot melt extrusion processing: review. Int J Pharm. 2020;576: 118989. https://doi.org/10.1016/j.ijpharm.2019.118989.

14. Forster A, Hempenstall J, Tucker I, Rades T. The potential of small-scale fusion experiments and the Gordon-Taylor equation to predict the suitability of drug/polymer blends for melt extrusion. Drug Dev Ind Pharm. 2001;27:549–60. https://doi.org/10.1081/DDC-100105180.

15. Zografi G, Newman A. Interrelationships between structure and the properties of amorphous solids of pharmaceutical interest. J Pharm Sci. 2017;106:5–27. https://doi.org/10.1016/j.xphs.2016.05.001.

16. Raman V, Sarabu S, Bandari S, Batra A, Bi V, Durig T, et al. Stable amorphous solid dispersions of fenofibrate using hot melt extrusion technology : effect of formulation and process parameters for a low glass transition temperature drug. J Drug Deliv Sci

17. Technol. 2020;58: 101395. https://doi.org/10.1016/j.jddst.2019.101395.

17. Wu J, Van den Mooter G. The influence of hydrogen bonding between different crystallization tendency drugs and PVPVA on the stability of amorphous solid dispersions. Int J Pharm. 2023. https://doi.org/10.1016/j.ijpharm.2023.123440.

18. Newman A, Zografi G. What are the important factors that influence API crystallization in miscible amorphous API–excipient mixtures during long-term storage in the glassy state? Mol Pharm. 2022;19:378–91. https://doi.org/10.1021/acs.molpharmaceut.1c00519.

19. Roudaut G, Simatos D, Champion D, Contreras-Lopez E, Le Meste M. Molecular mobility around the glass transition temperature: a mini review. Innov Food Sci Emerg Technol. 2004;5:127–34. https://doi.org/10.1016/j.ifset.2003.12.003.

20. Matsuo M, Bin Y, Xu C, Ma L, Nakaoki T, Suzuki T. Relaxation mechanism in several kinds of polyethylene estimated by dynamic mechanical measurements, positron annihilation, X-ray and 13C solid-state NMR. Polymer. 2003;44:4325–40. https://doi.org/10.1016/S0032-3861(03)00352-5.

21. Kissi EO, Grohganz H, Lo K, Ruggiero MT, Zeitler JA, Rades T. Glass-transition temperature of the β—relaxation as the major predictive parameter for recrystallization of neat amorphous drugs. J Phys Chem. 2018;122:2803–8. https://doi.org/10.1021/acs.jpcb.7b10105.

22. Sibik J, Löbmann K, Rades T, Zeitler JA. Predicting crystallization of amorphous drugs with terahertz spectroscopy. Mol Pharm. 2015;12:3062–8. https://doi.org/10.1021/acs.molpharmaceut.5b00330.

23. Grzybowska K, Chmiel K, Knapik-Kowalczuk J, Grzybowski A, Jurkiewicz K, Paluch M. Molecular factors governing the liquid and glassy states recrystallization of celecoxib in binary mixtures with excipients of different molecular weights. Mol Pharm. 2017;14:1154–68. https://doi.org/10.1021/acs.molpharmaceut.6b01056.

24. Jadhav NR, Gaikwad VL, Nair KJ, Kadam HM. Glass transition temperature: basics and application in pharmaceutical sector. Asian J Pharm. 2009;3:82. https://doi.org/10.4103/0973-8398.55043.

25. Leyva-Porras C, Cruz-Alcantar P, Espinosa-Solís V, Martínez-Guerra E, Piñón-Balderrama CI, Compean Martínez I, et al. Application of differential scanning calorimetry (DSC) and modulated differential scanning calorimetry (MDSC) in food and drug industries. Polymers. 2019;12:5. https://doi.org/10.3390/polym12010005.

26. Giron D. Applications of thermal analysis in the pharmaceutical industry. J Pharm Biomed Anal. 1986;4:755–70. https://doi.org/10.1016/0731-7085(86)80086-3.

27. Thayumanasundaram S, Venkatesan TR, Ousset A, Van Hollebeke K, Aerts L, Wübbenhorst M, et al. Complementarity of mDSC, DMA, and DRS techniques in the study of Tg and Sub-Tg transitions in amorphous solids: PVPVA, indomethacin, and amorphous solid dispersions based on indomethacin/PVPVA. Mol Pharm. 2022;19:2299–315. https://doi.org/10.1021/acs.molpharmaceut.2c00123.

28. Szabó E, Haraszti A, Záhonyi P, Vadas D, Csontos I, Nagy ZK, et al. Evaluation of different thermoanalytical methods for the analysis of the stability of naproxen-loaded amorphous solid dispersions. Pharmaceutics. 2022;14:2508. https://doi.org/10.3390/pharmaceutics14112508.

29. Baird JA, Taylor LS. Evaluation of amorphous solid dispersion properties using thermal analysis techniques. Adv Drug Deliv Rev. 2012;64:396–421. https://doi.org/10.1016/j.addr.2011.07.009.

30. Ramos JJM, Diogo HP. The determination of the glass transition temperature by thermally stimulated depolarization currents. Comparison with the performance of other techniques. Phase Transit. 2017;90:1061–78. https://doi.org/10.1080/01411594.2017.1320715.

31. Rodrigues AC, Viciosa MT, Danède F, Affouard F, Correia NT. Molecular mobility of amorphous S-Flurbiprofen: a dielectric relaxation spectroscopy approach. Mol Pharm. 2014;11:112–30. https://doi.org/10.1021/mp4002188.

32. Ramos JJM, Diogo HP. The slow relaxation dynamics in active pharmaceutical ingredients studied by DSC and TSDC: voriconazole, miconazole and itraconazole. Int J Pharm. 2016;501:39–48. https://doi.org/10.1016/j.ijpharm.2016.01.057.

33. Bertoldo Menezes D, Reyer A, Marletta A, Musso M. Determination of the temperatures of the γ, β and α relaxation processes in nylon 6,6 by Raman spectroscopy. Polymer. 2016;106:85–90. https://doi.org/10.1016/j.polymer.2016.10.058.

34. Liem H, Cabanillas-Gonzalez J, Etchegoin P, Bradley DDC. Glass transition temperatures of polymer thin films monitored by Raman scattering. J Phys Condens Matter. 2004;16:721–8. https://doi.org/10.1088/0953-8984/16/6/003.

35. Janssens S, De Zeure A, Paudel A, Van Humbeeck J, Rombaut P, Van den Mooter G. Influence of preparation methods on solid state supersaturation of amorphous solid dispersions: a case study with itraconazole and eudragit E100. Pharm Res. 2010;27:775–85. https://doi.org/10.1007/s11095-010-0069-y.

36. Baghel S, Cathcart H, O'Reilly NJ. Polymeric amorphous solid dispersions: a review of amorphization, crystallization, stabilization, solid-state characterization, and aqueous solubilization of biopharmaceutical classification system class II drugs. J Pharm Sci. 2016;105:2527–44. https://doi.org/10.1016/j.xphs.2015.10.008.

37. Six K, Verreck G, Peeters J, Brewster M, Van den Mooter G. Increased physical stability and improved dissolution properties of itraconazole, a class II drug, by solid dispersions that combine fast- and slow-dissolving polymers. J Pharm Sci. 2004;93:124–31. https://doi.org/10.1002/jps.10522.

38. Espeau P, Nicolaï B, Céolin R, Perrin MA, Zaske L, Giovannini J, et al. Thermal behavior of orthorhombic polymorphs I and II of spironolactone. J Therm Anal Calorim. 2007;90:341–2. https://doi.org/10.1007/s10973-007-8390-3.

39. Reddy R, Lucy CL, Luthra S, Collins G, Lopez C, Shamblin SL, et al. The glass transition and sub-Tg-relaxation in pharmaceutical powders and dried proteins by thermally stimulated current. J Pharm Sci. 2009;98:81–93. https://doi.org/10.1002/jps.21397.

40. Utracki LA, Wilkie CA (eds.), Polymer blends handbook, 2014.

41. Taylor LS, Langkilde FW, Zografi G. Fourier transform Raman spectroscopic study of the interaction of water vapor with amorphous polymers. J Pharm Sci. 2001;90:888–901. https://doi.org/10.1002/jps.1041.

42. Lin-Vien D, Colthup NB, Fateley WG, G.Grasselli J. The handbook of infrared and Raman characteristic frequencies of organic molecules. Academic Press; 1991.

43. Jubert A, Legarto ML, Massa NE, Tévez LL, Okulik NB. Vibrational and theoretical studies of non-steroidal anti-inflammatory drugs Ibuprofen [2-(4-isobutylphenyl)propionic acid]; Naproxen [6-methoxy-α-methyl-2-naphthalene acetic acid] and Tolmetin acids [1-methyl-5-(4-methylbenzoyl)-1H-pyrrole-2-acetic acid]. J Mol Struct. 2006;783:34–51. https://doi.org/10.1016/j.molstruc.2005.08.018.

44. Aßmann M, Stöbener A, Mügge C, Gaßmeyer SK, Hilterhaus L, Kourist R, et al. Reaction engineering of biocatalytic (S)-naproxen synthesis integrating in-line process monitoring by Raman spectroscopy. React Chem Eng. 2017;2:531–40. https://doi.org/10.1039/C7RE00043J.

45. Allesø M, Chieng N, Rehder S, Rantanen J, Rades T, Aaltonen J. Enhanced dissolution rate and synchronized release of drugs in binary systems through formulation: amorphous naproxen–cimetidine mixtures prepared by mechanical activation. J Control Release. 2009;136:45–53. https://doi.org/10.1016/j.jconrel.2009.01.027.